

Supporting Information

Defect Engineering in MIL-125-(Ti)-NH₂ for Enhanced Photocatalytic H₂ Generation

Ladawan Pukdeejorhor,^a Suttipong Wannapaiboon,^b Jan Berger,^c Katia Rodewald,^d Sutarat Thongratkaew,^e Sarawoot Impeng,^e Julien Warnan,^{,c} Sareeya Bureekaew,^a Roland A. Fischer,^{*,c}*

^aSchool of Energy Science and Engineering, Vidyasirimedhi Institute of Science and Technology, 555 Moo 1 Payupnai, Wangchan, Rayong 21210, Thailand.

^bSynchrotron Light Research Institute, 111 University Avenue, Muang, Nakhon Ratchasima 30000, Thailand.

^cTUM School of Natural Sciences, Department of Chemistry, Chair of Inorganic and Metal-Organic Chemistry; Catalysis Research Center (CRC), Technical University of Munich, Lichtenbergstrasse 4, 85748 Garching, Germany.

^dWacker-Chair of Macromolecular Chemistry, Catalysis Research Centre, Ernst Otto-Fischer Strasse 1 and Department of Chemistry, Technical University of Munich, Lichtenbergstrasse 4, 85747 Garching b. München, Germany.

^eNational Nanotechnology Center (NANOTEC), National Science and Technology Development Agency (NSTDA), 111 Thailand Science Park, Pahonyothin Rd., Klong Luang, Pathumthani 12120, Thailand.

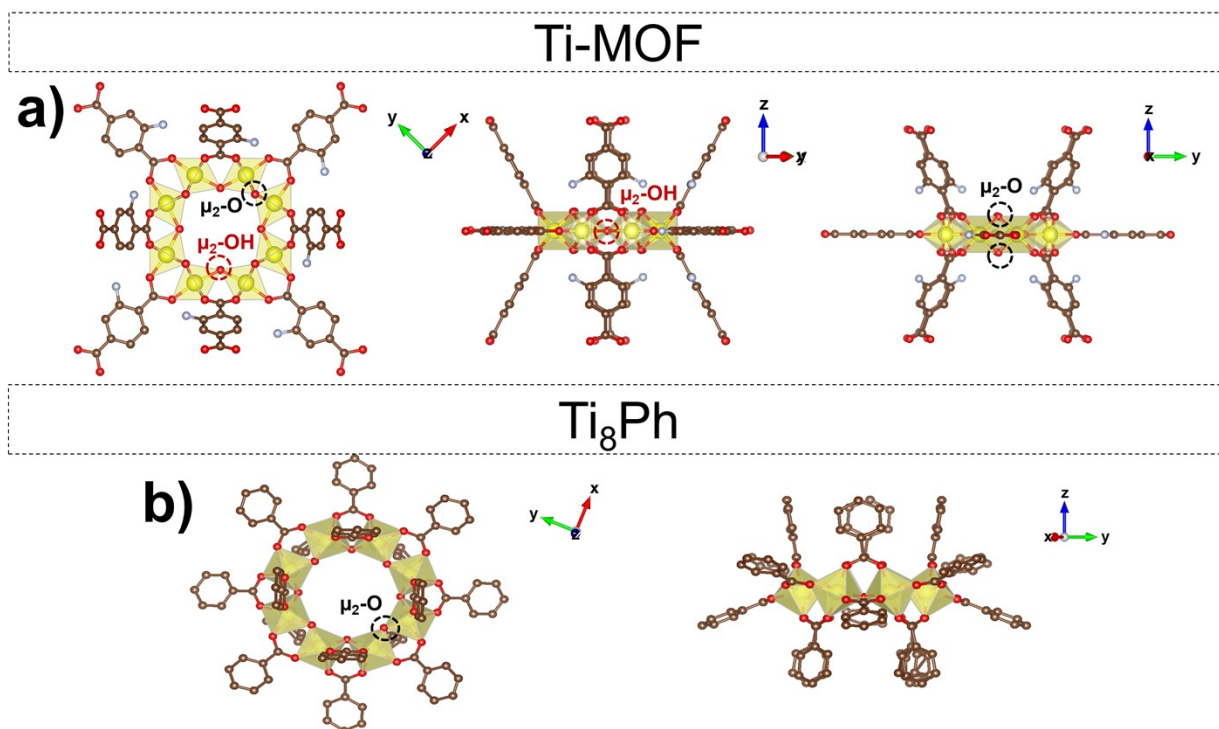


Figure S1. Cluster of a) Ti-MOF and b) Ti₈Ph. Ti; yellow, O; red, C; brown, N; light blue, H atoms are omitted for clarity.

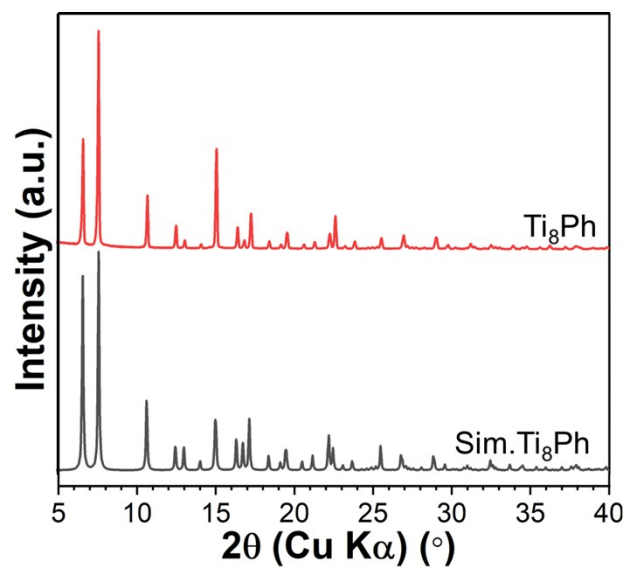


Figure S2. PXRD patterns of as-synthesized Ti₈Ph and simulated Ti₈Ph.

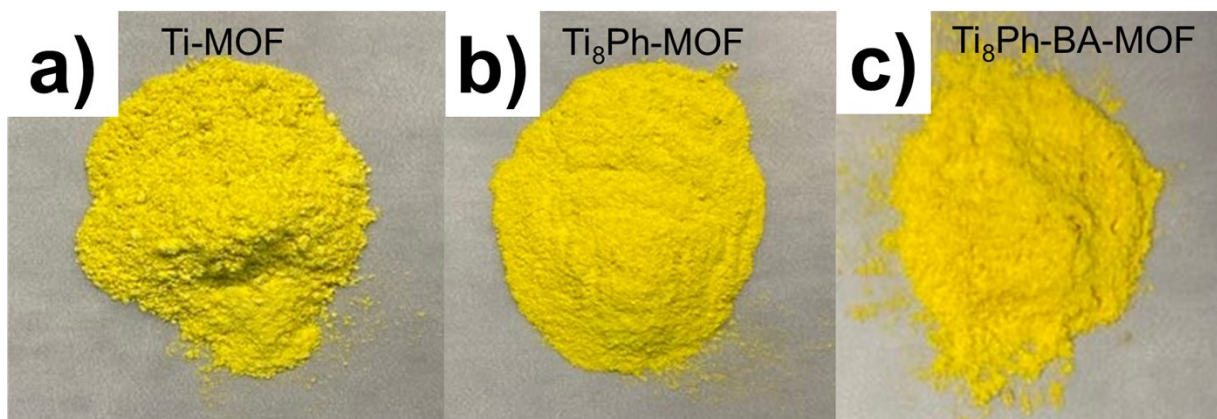


Figure S3. Photographs of a) Ti-MOF, b) Ti₈Ph-MOF, and c) Ti₈Ph-BA-MOF.

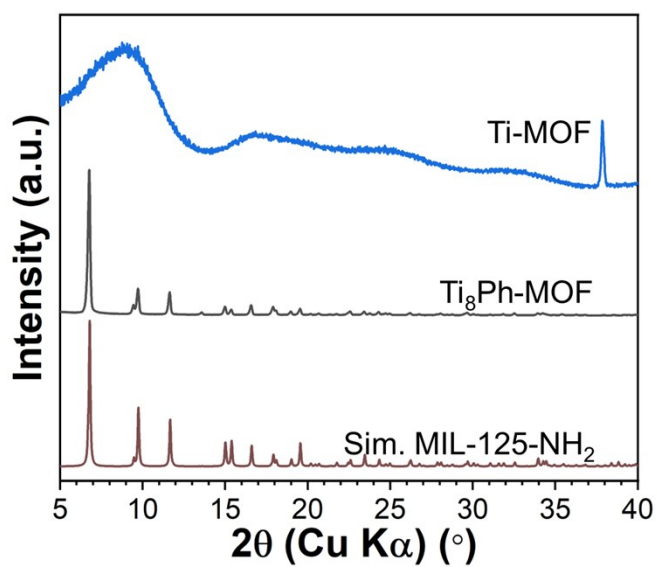


Figure S4. PXRD patterns of Ti-MOF, and Ti₈Ph-MOF synthesized at 70 °C as compared with the simulated reference of MIL-125-NH₂.

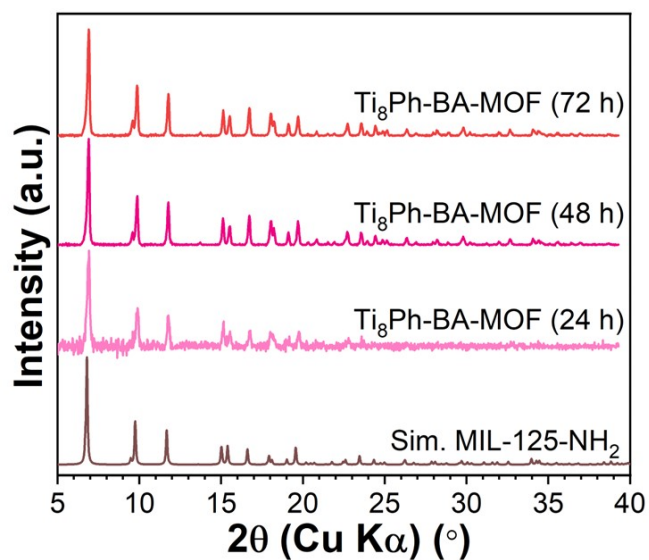


Figure S5. PXRD patterns of $Ti_8Ph-BA-MOF$ synthesized at 70 $^\circ C$ for 24, 48, and 72 h.

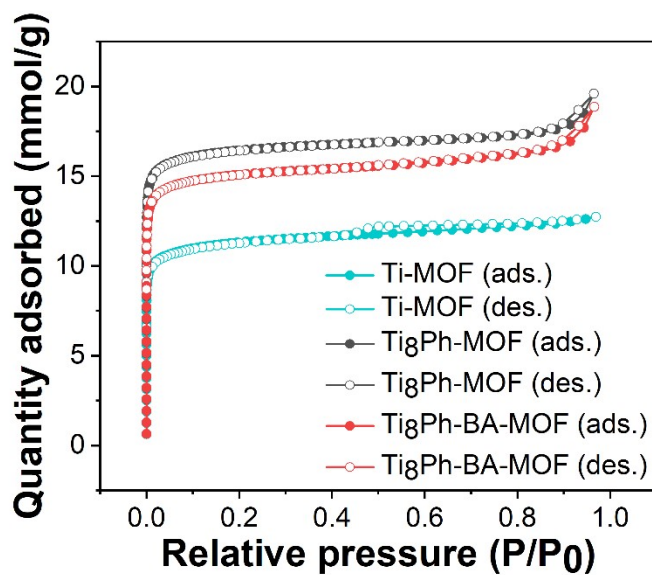


Figure S6. N_2 (99.999%) adsorption–desorption isotherms at 77 K, of $Ti-MOF$, $Ti_8Ph-MOF$, and $Ti_8Ph-BA-MOF$. Free space of the sample tube was determined prior to measuring each isotherm using helium (99.999%).

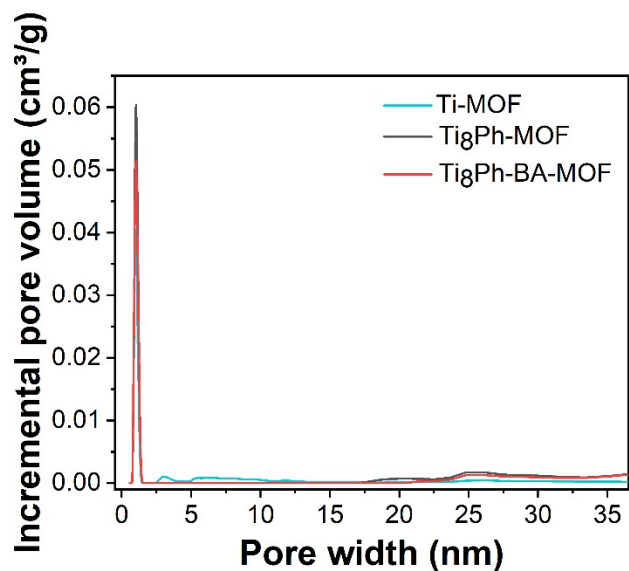


Figure S7. Pore size distributions for Ti-MOF, Ti₈Ph-MOF, and Ti₈Ph-BA-MOF. Distributions were derived by fitting the N₂ isotherms with sets of calculated isotherms (kernel) derived from non-local DFT (NLDFIT) based methods. Fitting was done via the 3Flex Software Version 5.01 by Micromeritics Instrument Corp. using a kernel for cylindrical pores ('oxide cyl pores, strong potential') provided with the software.

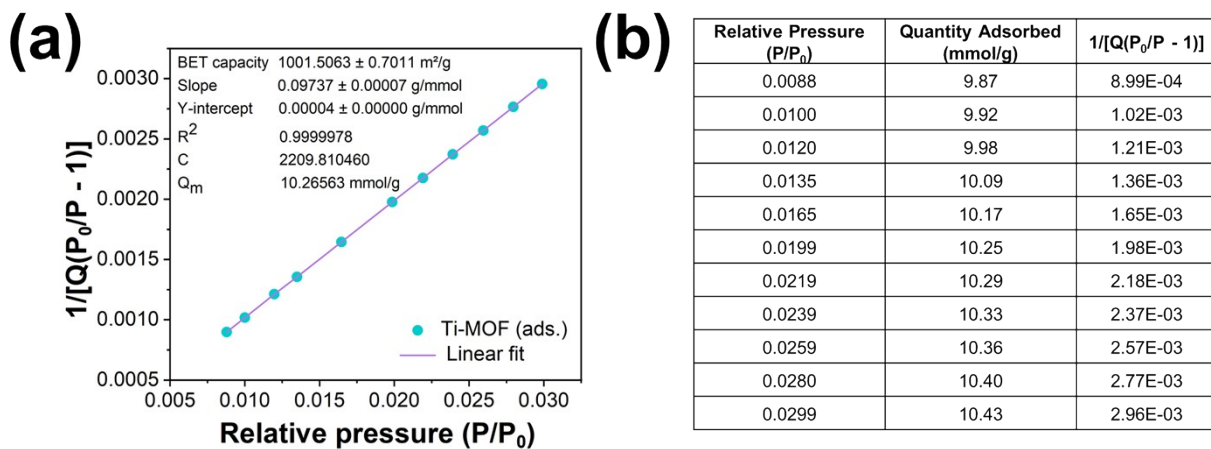


Figure S8. a) BET plot with linear fit control parameters and calculated monolayer capacity (Q_m), and b) Tabular BET plot data including amounts adsorbed in mmol/g for reference of Q_m for Ti-MOF.

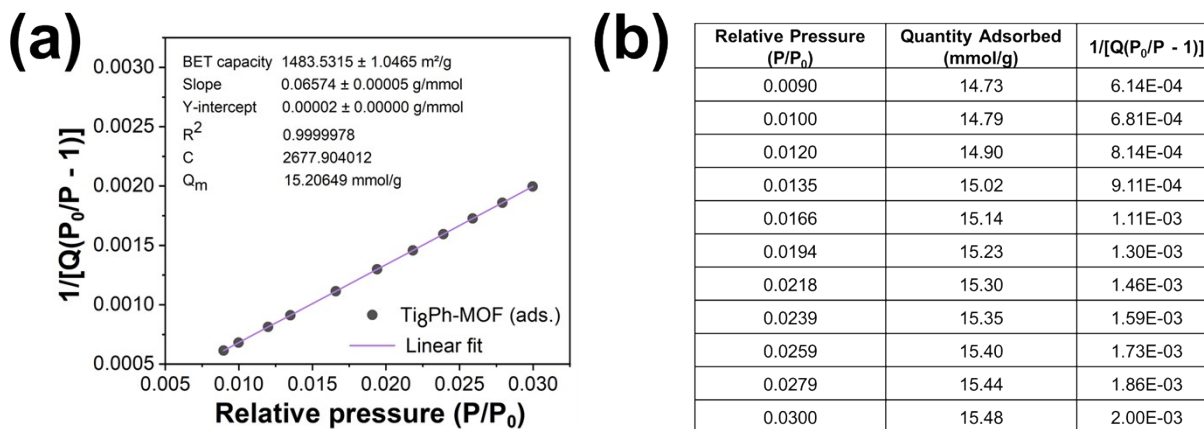


Figure S9. a) BET plot with linear fit control parameters and calculated monolayer capacity (Q_m), and b) Tabular BET plot data including amounts adsorbed in mmol/g for reference of Q_m for Ti₈Ph-MOF.

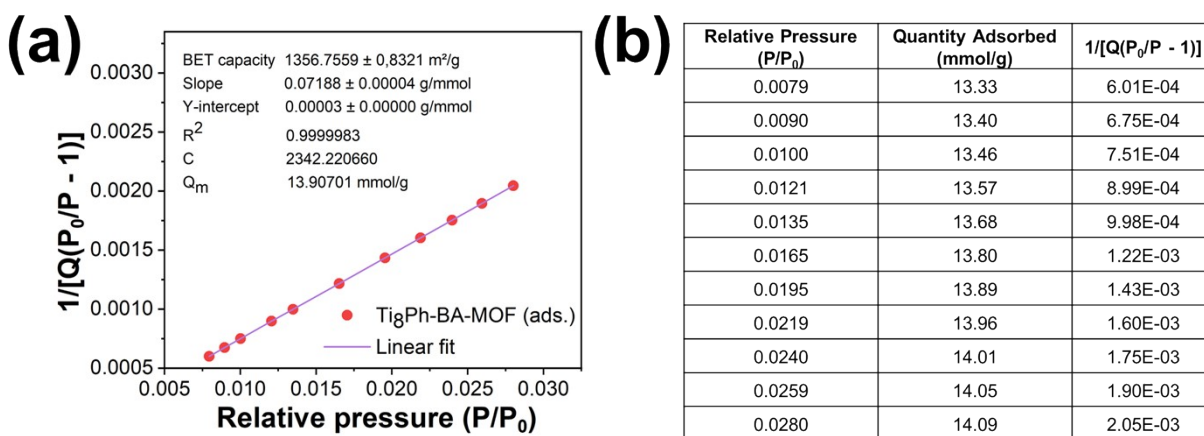


Figure S10. a) BET plot with linear fit control parameters and calculated monolayer capacity (Q_m), and b) Tabular BET plot data including amounts adsorbed in mmol/g for reference of Q_m for Ti₈Ph-BA-MOF.

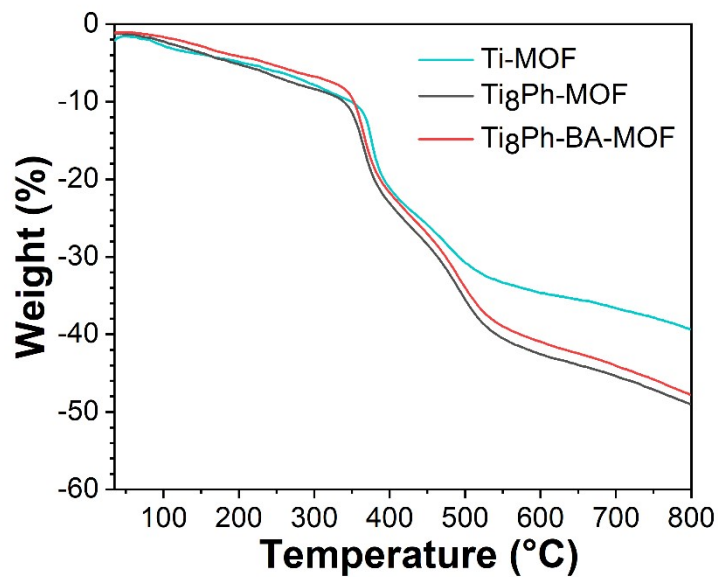


Figure S11. TGA curves of Ti-MOF, Ti₈Ph-MOF, and Ti₈Ph-BA-MOF after activation under Ar atmosphere.

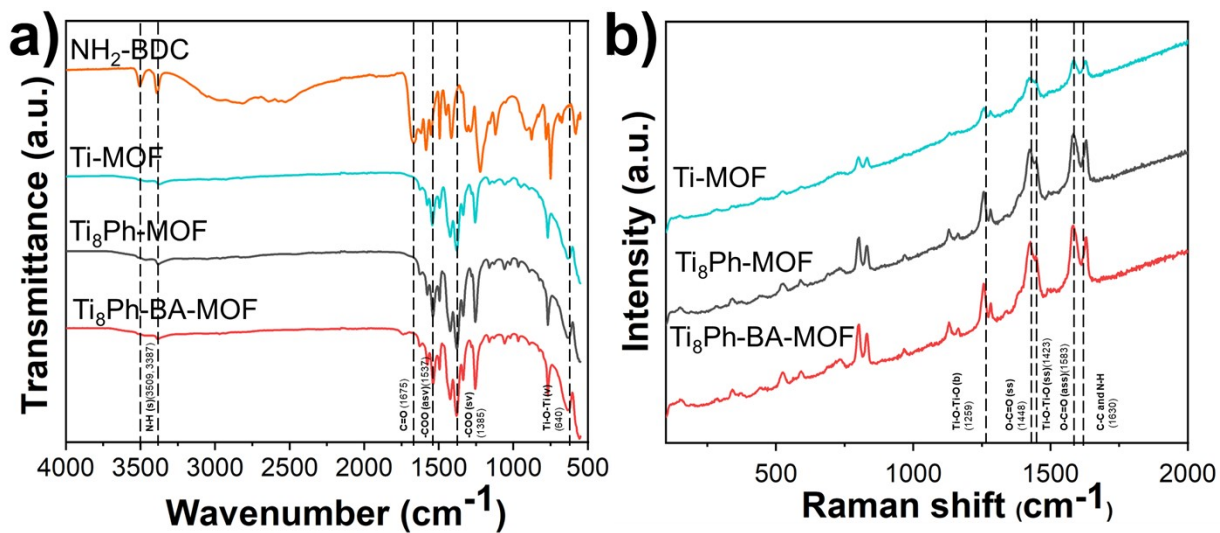


Figure S12. Overlaid a) IR and b) Raman spectra of Ti-MOF, Ti₈Ph-MOF, and Ti₈Ph-BA-MOF.

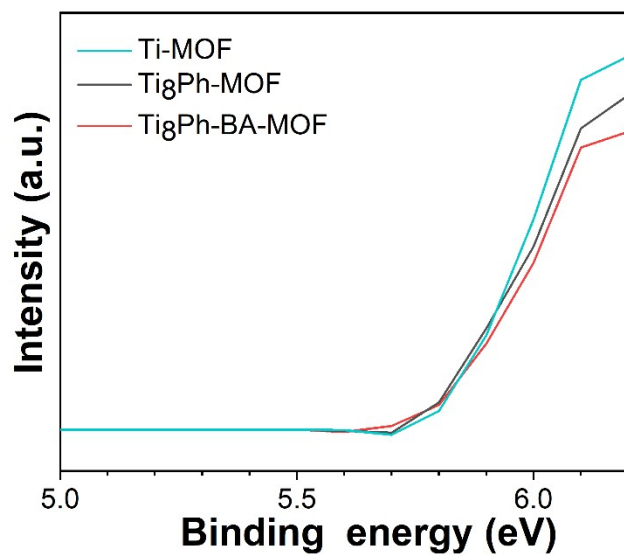


Figure S13. UPS spectra of Ti-MOF, $\text{Ti}_8\text{Ph-MOF}$, and $\text{Ti}_8\text{Ph-BA-MOF}$.

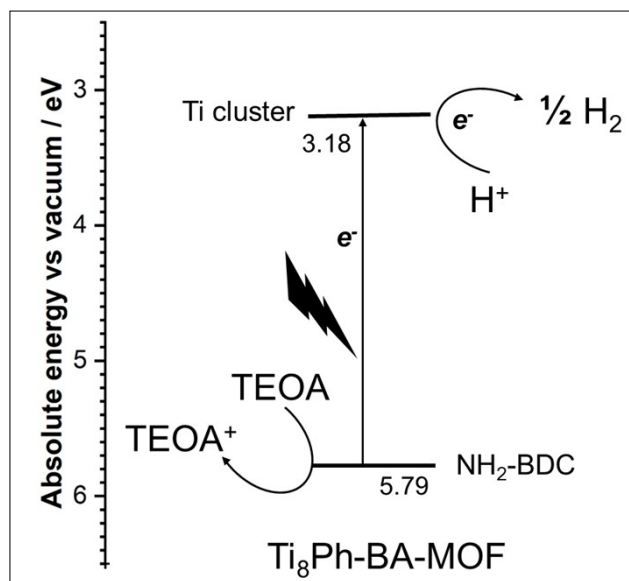


Figure S14. Schematic diagram of energy levels of component of $\text{Ti}_8\text{Ph-BA-MOF}$.

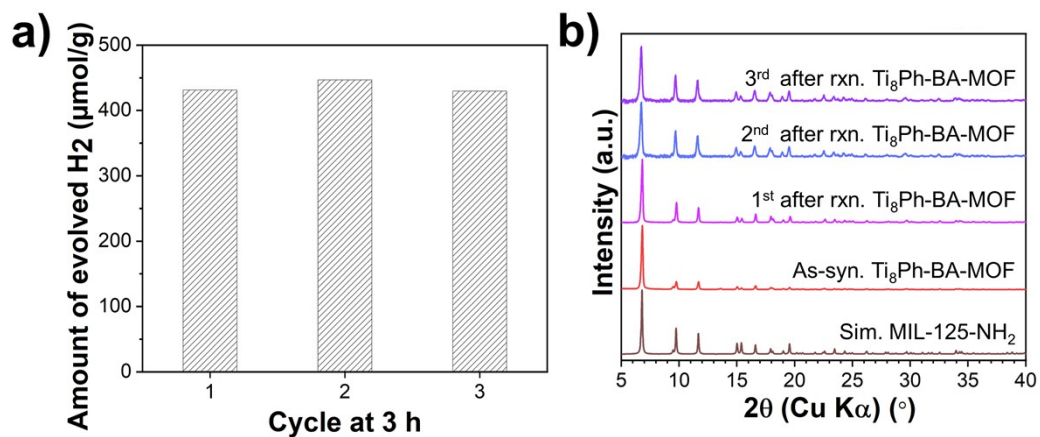


Figure S15. a) Result of photocatalytic reactions and b) PXRD patterns of recycling tests on $Ti_8Ph-BA-MOF$ with re-addition of 1.25 mL TEOA, 1 mL H_2O , and 22.75 mL CH_3CN .

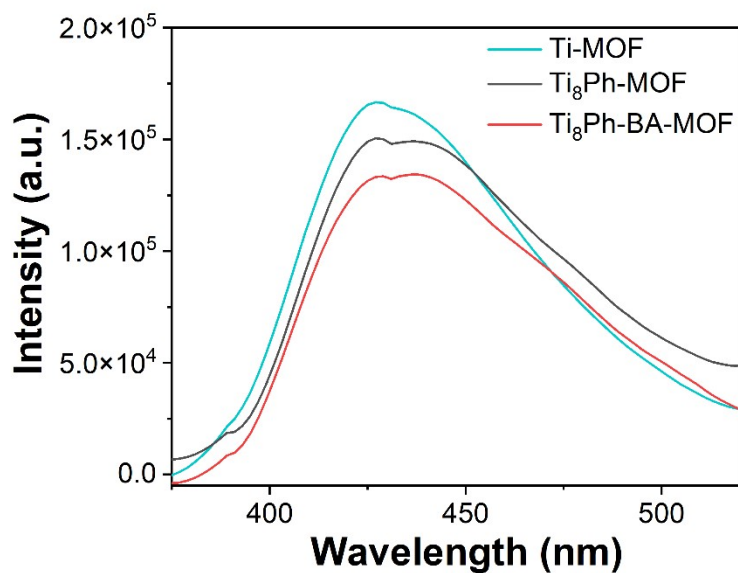


Figure S16. Photoluminescence spectra of $Ti-MOF$, $Ti_8Ph-MOF$, and $Ti_8Ph-BA-MOF$ (excited at 370 nm).

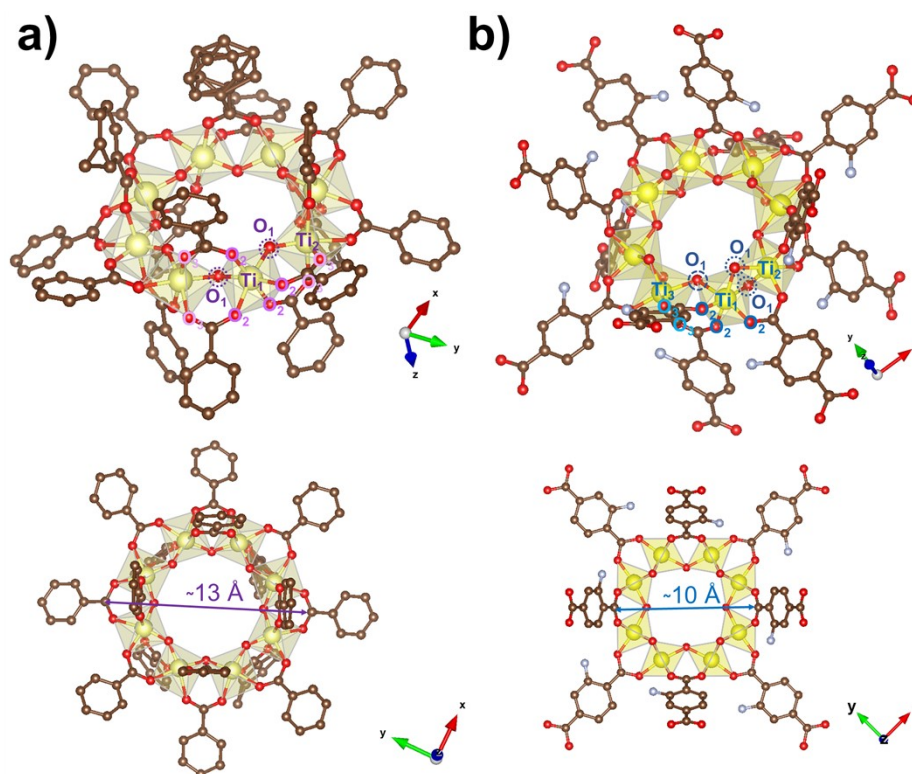


Figure S17. Model used for EXAFS analysis derived from local coordination environment of a) Ti_8Ph cluster and b) MIL-125- NH_2 (Ti-MOF). Ti; yellow, O; red, C; brown, N; light blue, H atoms are omitted for clarity. O_1 , O_2 , and O_3 in Ti_8Ph cluster presented μ_2 -O at the 1st shell, $\text{O}_{\text{the carboxylate group of linkers at the 1st shell}}$, and $\text{O}_{\text{the carboxylate group of linkers at the 3rd shell}}$ from Ti_1 centre, respectively. Ti-MOF, O_1 and O_2 presented both μ_2 -O & μ_2 -OH at the 1st shell and $\text{O}_{\text{the carboxylate group of linkers at the 1st shell}}$ from Ti_1 centre. O_3 revealed $\text{O}_{\text{the carboxylate group of linkers at the 3rd shell}}$.

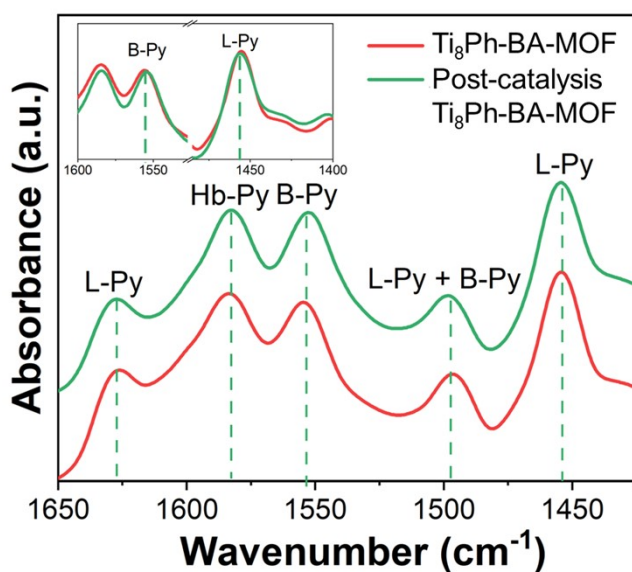


Figure S18. DRIFT spectra of pyridine of $\text{Ti}_8\text{Ph-BA-MOF}$ before and after reaction. Inset: High magnification presented the relative ratio of L-Py at 1454 cm^{-1} to B-Py at 1560 cm^{-1} . DRIFT spectra of pyridine of used sample were found similar to the fresh catalyst which indicates structural durability under photocatalysis condition.

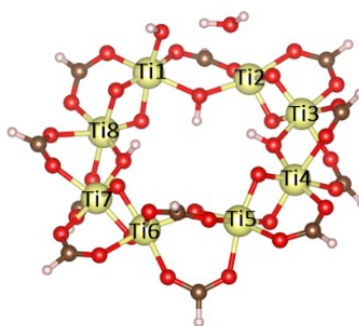


Figure S19. $\text{Ti}_8\text{O}_8(\text{OH})_4(\text{COOH})_{11}(\text{H}_2\text{O})_1(\text{OH})_1$ cluster model.

To investigate the reaction mechanism, the Ti-oxide cluster model representing the active site was taken from the crystal structure of MIL-125(Ti)- NH_2 .¹ To simulate the missing linker defect, one carboxylate linker, BDC- NH_2 was removed from the cluster. H_2O and hydroxide (OH^-) were then placed at the defect site with the intention of neutralizing the charge. To minimize computational expenses, all remaining BDC- NH_2 linkers were replaced with formate. The resultant Ti-oxide cluster with the formula $\text{Ti}_8\text{O}_8(\text{OH})_4(\text{COOH})_{11}(\text{H}_2\text{O})_1(\text{OH})_1$ (as illustrated in Figure S19) was used as the catalyst model to represent the missing linker defect in MIL-125(Ti)- NH_2 .

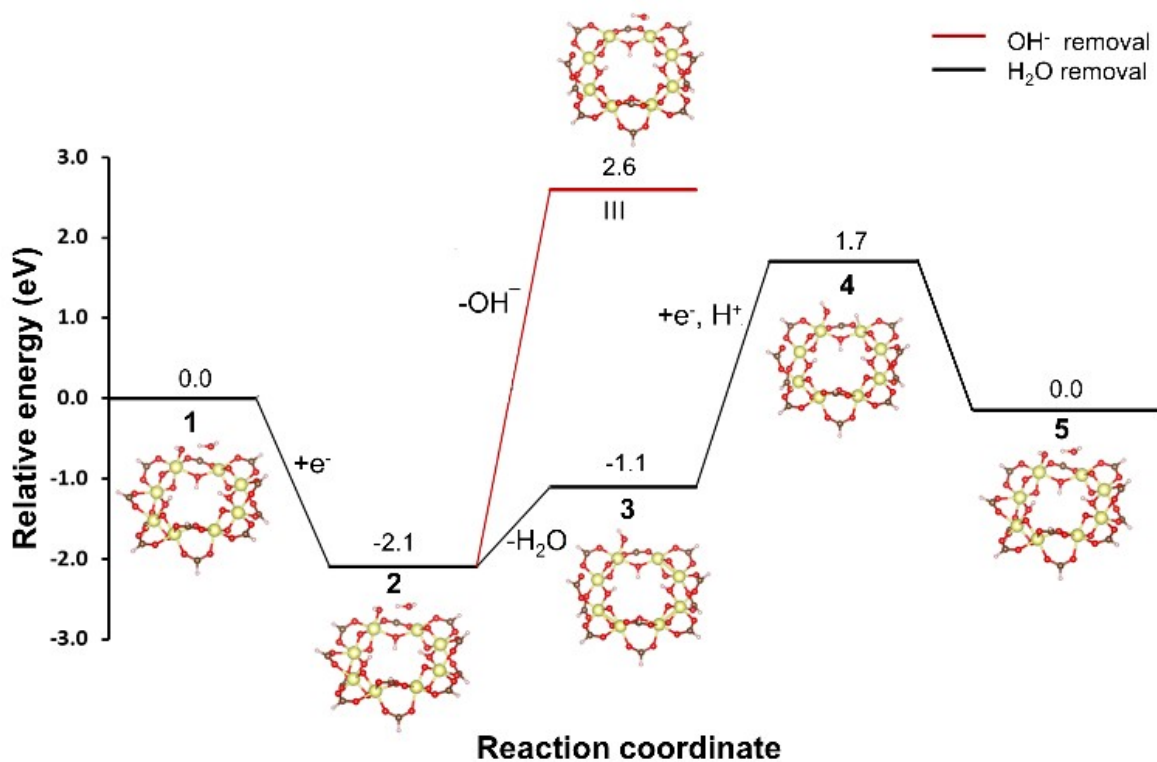


Figure S20. Energy profile for HER.

Table S1. Sorption Data of Ti-MOF, Ti₈Ph-MOF, and Ti₈Ph-BA-MOF

| Sample | S_{BET} (m ² /g) ^a | V_{micro} (cm ³ /g) ^b | V_{total} (cm ³ /g) |
|---------------------------|---|--|---|
| Ti-MOF | 1001.51 ± 0.70 | 0.36 | 0.39 |
| Ti ₈ Ph-MOF | 1483.53 ± 1.05 | 0.54 | 0.56 |
| Ti ₈ Ph-BA-MOF | 1356.76 ± 0.83 | 0.49 | 0.50 |

^a BET surface areas were calculated by applying the BET model and Rouquerol criteria. ^b Micropore and total pore volume were calculated using a NLDFT kernel (see Figure S5).

Table S2. VBM levels (measured by UPS) and energy gaps (obtained via Tauc's plot) for Ti-MOF, Ti₈Ph-MOF, and Ti₈Ph-BA-MOF.

| Sample | Energy gap (eV) | VBM level (eV) | CBM level (eV) ^a |
|---------------------------|-----------------|----------------|-----------------------------|
| Ti-MOF | 2.81 | 5.80 | 2.99 |
| Ti ₈ Ph-MOF | 2.63 | 5.79 | 3.16 |
| Ti ₈ Ph-BA-MOF | 2.61 | 5.79 | 3.18 |

^a Levels were estimated per MOF upon subtracting the energy gap to the VBM.

Table S3. Selected reports for photocatalytic hydrogen evolution reaction under visible light irradiation.

| Sample | Solvent | Electron source | Light Source | H ₂ (μmol/g/h) | Ref. |
|---|---------------------------------------|---|-------------------------------|---------------------------|-----------|
| CdS | H ₂ O | Lactic acid | 500 W Xe lamp (> 420 nm) | ~150 | [2] |
| | H ₂ O | Na ₂ S + Na ₂ SO ₃ | 350 W Xe lamp (> 400 nm) | ~60 | [3] |
| N-doped TiO ₂ P25 | H ₂ O | Formic acid | 15 W visible fluorescent lamp | ~10 | [4] |
| Cu ²⁺ -porphyrin MOF | H ₂ O | Ascorbic acid | 300 W Xe lamp (> 420 nm) | ~2 | [5] |
| Porphyrin Ti-MOF | H ₂ O | Ascorbic acid | 300 W Xe lamp (> 420 nm) | - | [6] |
| MIL-100(Fe) | H ₂ O | MeOH | 300 W Xe lamp (> 420 nm) | ~6 | [7] |
| MIL-101(Cr)-NH ₂ | H ₂ O | TEOA | 500 W Xe lamp (> 420 nm) | - | [8] |
| MIL-101(Cr)-NH ₂ + RuN ₃ ^a (dye) | | | | ~60 | |
| Co-ZIF-67 | CH ₃ CN + H ₂ O | TEOA | blue LED (405nm) | - | [9] |
| Co-ZIF-67 + RhB ^b (dye) | | | | ~10 | |
| UiO-66(Zr)-NH ₂ | CH ₃ CN + H ₂ O | TEA | 500 W Xe/Hg lamp (> 385 nm) | ~1 | [10] |
| defective UiO-66(Zr)-NH ₂ | | | | ~2 | |
| MIL-125(Ti)-NH ₂ | CH ₃ CN + H ₂ O | TEOA | 300 W Xe lamp (>380 nm) | ~20 | [11] |
| Ti ₈ Ph-BA-MOF | CH ₃ CN + H ₂ O | TEOA | 300 W Xe lamp (430-740 nm) | ~150 | This Work |

^a(cis-diisothiocyanato-bis (2,2'-bipyridyl-4,4'-dicarboxylic acid) ruthenium(II)).^bRhodamine B.**Table S4** The HOMO and LUMO, at the isosurface values of 0.03 of the intermediate species along the HER pathway.

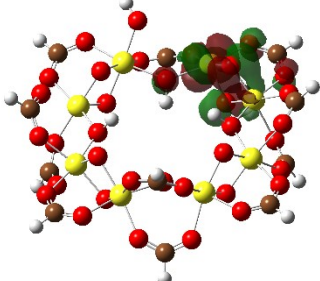
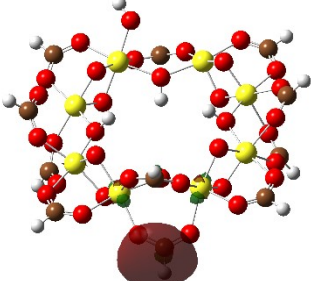
| System | Leve of calculations: MP2-6-31G**/LANL2DZ(Ti) | |
|--------|---|--|
| | HOMO | LUMO |
| 3 |  |  |

Table S5 Mulliken charges and spin densities ($\rho_\alpha - \rho_\beta$) calculated at MP2-6-31G**/LANL2DZ level of theory of Ti of Ti-OH and Ti-OH₂ of the intermediate species along the HER pathway.

| System | Charge (e) | | Spin density ($\rho_\alpha - \rho_\beta$) | |
|--------|---------------------|--------------------|---|-----------------------|
| | MP2-6-31G**/LANL2DZ | | MP2-6-31G**/LANL2DZ | |
| | Ti-OH | Ti-OH ₂ | Ti-OH | Ti-OH ₂ |
| 1 | 2.27 | 2.30 | - | - |
| 2 | 2.27 | 2.27 | 0.00 | 0.00 (Ti5 = 0.98)* |
| 3 | 2.22 | 1.90 | 0.00 | 1.00 |
| III | 1.31 | 2.31 | - | - |
| 4 | 2.23 | 1.94 | - | - |

*Ti5 as shown in Figure S19

References

- [1] A. P. Smalley, D. G. Reid, J. C. Tanb and G. O. Lloyd, *CrystEngComm*, 2013, **15**, 9368-9371.
- [2] X. Zong, H. Yan, G. Wu, G. Ma, F. Wen, L. Wang and C. Li, *J. Am. Chem. Soc.*, 2008, **130**, 7176–7177.
- [3] J. Yu, J. Zhanga and M. Jaroniec, *Green Chem.*, 2010, **12**, 1611-1614.
- [4] K. Villa, A. Black, X. Domenech and J. Peral, *Sol. Energy*, 2012, **86**, 558-566.
- [5] Q. Zuo, T. Liu, C. Chen, Y. Ji, X. Gong, Y. Mai and Y. Zhou, *Angew. Chem., Int. Ed.*, 2019, **58**, 10198-1020.
- [6] X. Wang, X. Zhang, W. Zhou, L. Liu, J. Ye and D. Wang, *Nano Energy*, 2019, **62**, 250-258.
- [7] D. Wang, Y. Song, J. Cai, L. Wu and Z. Li, *New J. Chem.*, 2016, **40**, 9170-9175.
- [8] M. Wen, K. Mori, T. Kamegawaab and H. Yamashita, *Chem. Commun.*, 2014, **50**, 11645-1164.
- [9] S. Yang, B. Pattengale, E. L Kovrigin and J. Huang, *ACS Energy Lett.*, 2017, **2**, 75-80.
- [10] M. A. Nasalevich, C. H. Hendon, J. G. Santaclara, K. Svane, B. van der Linden, S. L. Veber, M. V. Fedin, A. J. Houtepen, M. A. van der Veen, F. Kapteijn, A. Walsh and J. Gascon, *Sci. Rep.*, 2016, **6**, 23676.
- [11] Z. Li, J. D. Xiao and H. L. Jiang, *ACS Catal.*, 2016, **6**, 5359-5365